

Original Research Article

Structural and Electronic Properties of Hexagonal $Y_{1-x}Eu_xMnO_3$

ABSTRACT

Magnetolectric materials attract interest due to coupling between the magnetic and dipole moments, which provides additional degrees of freedom in magnetolectric device design and nanotechnological applications. Despite intensive theoretical and experimental studies already carried out in magnetolectric materials, some issues deserve more attention, specifically their structural and electronic properties. Here, we use density functional theory (DFT) was used to investigate the structural and electronic properties of hexagonal $Y_{1-x}Eu_xMnO_3$ ($x = 0.0, 0.1$ and 0.2) compounds. Our approach is based on the local spin density approximation (LSDA+U). The magnetic moment carried by Mn atoms is very sensitive to the LSDA+U. We obtain the lattice parameters that compare well with experimental X-ray measurements, with the difference between calculated values and experiment being less than 2%. In addition, the electronic partial density of states (PDOS) shows a dominant contribution from the Mn and rare earth atoms near the Fermi level.

Keywords: Magnetolectric; Ab-initio; Hexagonal and Ceramic.

1. INTRODUCTION

A major current technological thrust is based on the development and optimization of new materials, in particular multiferroic compounds and heterostructures, since they exhibit a strong coupling in magnetic and polar degrees of freedom (the so called magnetolectric effect) [1]. Magnetolectric materials have attracted a lot of interest, as the coupling between the magnetization and electric polarization provides an additional degree of freedom in magnetolectric device design [2, 3].

In previous work, we studied a system of manganites, called $Eu_{1-x}Y_xMnO_3$, leading to great interest in these compounds [4], but we examined only its orthorhombic regime (Pbn structure). Hexagonal manganites are few despite their interesting properties. Magnetic ordering occurs in both the orthorhombic and the hexagonal phase, but the hexagonal regime is more interesting due to ferroelectricity in the non-centrosymmetric $P6_3cm$ phase group, in which the rich yttrium content $Y_{1-x}Eu_xMnO_3$ ceramics crystallize. Unlike the orthorhombic case, there are practically no reported investigations on hexagonal $Y_{1-x}Eu_xMnO_3$ compounds.

The small ionic radius of Y^{3+} results in a small value of the tolerance factor, leading to an instability of the perovskite structure [5]. Under standard preparation conditions, $YMnO_3$ crystallizes in a hexagonal structure unrelated to the perovskites. However, the metastable $YMnO_3$ orthorhombic perovskite phase can be stabilized by high pressure synthesis or by changing the average ionic radius of the Y site, i.e., by partial substitution of yttrium (Y) by europium (Eu) [6].

The hexagonal YMnO_3 ceramics system displays antiferromagnetic order below a Néel temperature of 80 K, and a para-ferroelectric phase transition at 914 K. The couplings observed in this material have a realistic potential for practical applications in electronic devices, where the dielectric (capacitive) response can be changed by the onset of the magnetic transition or by application of an external magnetic field [7].

In this paper, we carry out a systematic study of YMnO_3 , $\text{Y}_{0.9}\text{Eu}_{0.1}\text{MnO}_3$, and $\text{Y}_{0.8}\text{Eu}_{0.2}\text{MnO}_3$ using density functional theory and X-ray diffraction.

2. METHODOLOGY

The electronic properties of $\text{Y}_{1-x}\text{Eu}_x\text{MnO}_3$ were obtained by optimizing the structures using the density functional theory (DFT) approach [8, 9]. The systems crystallize in a hexagonal structure with space group $\text{P6}_3\text{cm}$ (see Fig. 1). The periodic DFT calculations were performed using the plane-wave pseudopotential method, as implemented in the CASTEP code [10]. The calculations were carried out by spin-polarized DFT within the local spin density approximation (LSDA+U), suitable for transition metal oxides, certain inorganic surface studies, and metallic systems containing magnetic elements, as presented in Ref. [11]. The exchange correlation was calculated using the Perdew-Zunger parametrization [12] of the Ceperley-Alder potential [13]. For geometry optimization, ultrasoft Vanderbilt-type pseudopotentials [14] were used, considering the following electronic configurations for each atomic species: Eu- $4f^7-5s^2-5p^6$, Y- $4s^2-4p^6-4d^1-5s^2$, Mn- $3d^5-4s^2$, and O- $2s^2-2p^4$ within the virtual crystal approximation (VCA) implemented in the CASTEP code [15], which is used to model disorder in solids. VCA calculations use weights according to the site occupancies to obtain the contribution of each pseudopotential. A Monkhorst-Pack [16] $3 \times 3 \times 2$ sampling was used to evaluate all integrals in reciprocal space, its grid being selected to ensure a well converged electronic structure for each crystal.

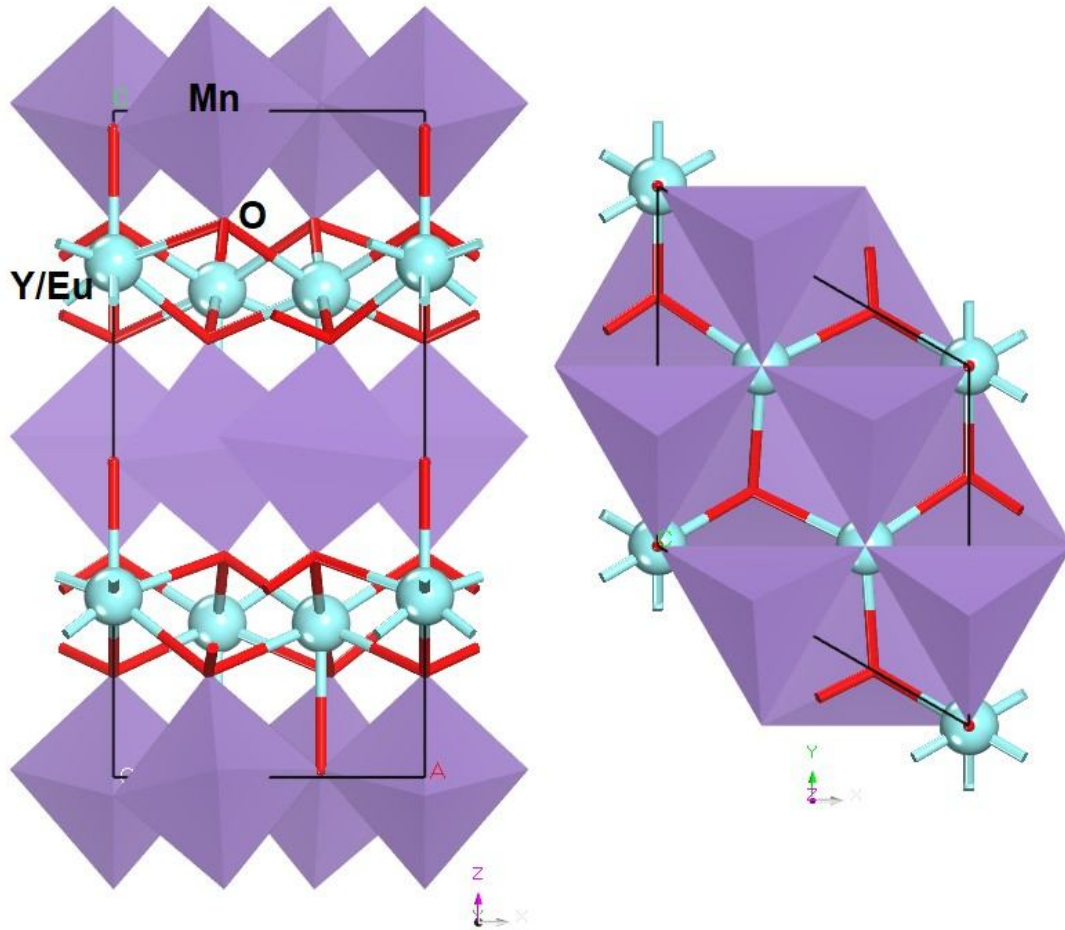


Fig. 1. Hexagonal crystal structure of $Y_{1-x}Eu_xMnO_3$.

Lattice parameters and atomic positions were optimized by seeking a total minimum energy for the $Y_{1-x}Eu_xMnO_3$ unit cell. The convergence tolerances for all geometry optimizations were: total energy change smaller than 0.5×10^{-5} eV/atom, maximum force per atom below 0.1×10^{-1} eV/Å, pressure smaller than 0.02 GPa, and maximum atomic displacement not exceeding 0.5×10^{-3} Å. The convergence tolerance window was for two successive steps, and the optimization method used Broyden-Fletcher-Goldfarb-Shanno (BFGS) minimization [17], which is used to perform cell optimization, including optimization at fixed external stress. The BFGS scheme uses a starting Hessian which is recursively updated during optimization. Within each self-consistent field (SCF) step, the electronic minimization parameters for convergence were: total energy/atom smaller 5×10^{-7} eV/atom, electronic eigen-energy variation smaller than 0.1071×10^{-6} eV at most, and a convergence window of three SCF cycles. A plane-wave basis set was adopted to represent the Kohn-Sham orbitals, with cutoff energy chosen, after convergence studies, to be 880 eV. The quality of this basis set was kept fixed even taking into account the unit cell volume variations during the geometry optimization process. After obtaining the optimized unit cells and atomic positions, the Kohn-Sham electronic band structure and the partial density of states (PDOS) were evaluated for the optimized LSDA unit cell.

3. RESULTS AND DISCUSSION

3.1 Crystal Structure at Room Temperature

Room temperature X-ray powder diffraction (XRD) spectra obtained from the system, are displayed in Fig. 2. Here, $x = 1$, $x = 0.1$, and $x = 0.2$ correspond to YMnO_3 , $\text{Y}_{0.9}\text{Eu}_{0.1}\text{MnO}_3$, and $\text{Y}_{0.8}\text{Eu}_{0.2}\text{MnO}_3$, respectively. No secondary crystallographic phases were detected.

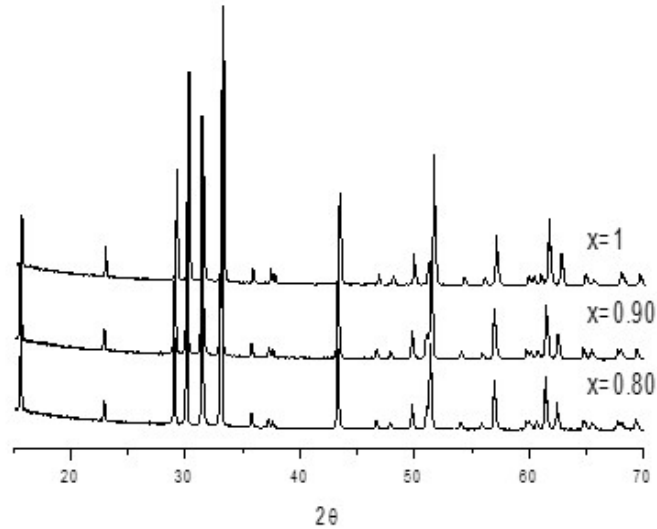


Fig. 2. X-ray diffraction spectra of $\text{Y}_{1-x}\text{Eu}_x\text{MnO}_3$ recorded at room temperature.

The samples were prepared using the urea sol-gel combustion method. Stoichiometric amounts of Eu_2O_3 (Alfa Aesar, chemical purity), Y_2O_3 (Aldrich, 99.99%), and $\text{Mn}(\text{NO}_3)_2 \cdot 4\text{H}_2\text{O}$ (ABCR chemical purity) were dissolved in diluted aqueous solution of nitric acid.

Hexagonal $\text{Y}_{1-x}\text{Eu}_x\text{MnO}_3$ consists of MnO_5 trigonal bipyramids where each manganese ion is surrounded by three in-plane and two apical oxygen ions and presents corner linked to form a triangular-lattice layer in the ab -plane. The Mn-O1 and Mn-O2 bonds are parallel to the c -axis, and the triangular base of MnO_5 bipyramids is vertical to the c -axis.

Table 1 shows the values of the cell parameters and density obtained from the structural refinement of the XRD data.

Table 1. Cell parameters and density obtained from the analysis of the XRD spectra.

	$\text{Y}_{0.8}\text{Eu}_{0.2}\text{MnO}_3$	$\text{Y}_{0.9}\text{Eu}_{0.1}\text{MnO}_3$	YMnO_3
$a(\text{\AA})$	6.1663	6.155	6.1404
$c(\text{\AA})$	11.3985	11.3990	11.3967
$V(\text{\AA}^3)$	375.289	373.999	372.14
$\rho(\text{g/cm}^3)$	4.968	4.990	4.470

3.2 Geometry Optimization

LDA lattice parameters, almost always, are smaller than experimental measured ones due to the well-known trend of this functional to overestimate the strength of interatomic interactions, while the calculations were carried out by spin-polarized DFT calculations.

Table 2 presents a comparison of the experimental lattice parameters and cell volumes and the corresponding values obtained from DFT-LSDA+U computations. The deviations between the experimental and calculated values are also presented.

Table 2. Lattice parameters for $Y_{1-x}Eu_xMnO_3$ after DFT-LSDA computations. Experimental data (EXP.) for $YMnO_3$ ($x = 1$), $Y_{0.8}Eu_{0.2}MnO_3$ ($x=0.2$) and $Y_{0.9}Eu_{0.1}MnO_3$ ($x=0.1$), respectively.

Alloy/Data Source	$a(\text{\AA})$	$b(\text{\AA})$	$c(\text{\AA})$	$V(\text{\AA}^3)$
LSDA ($x=1$)	6.0514 (-1.4%)	6.0514 (-1.4%)	11.4284 (+0.2%)	362.43 (-2.6%)
<i>Exp</i> ($x=1$)	6.1404	6.1404	11.3967	372.14
LSDA ($x=0.2$)	6.0657 (-1.4%)	6.0657 (-1.4%)	11.4635 (+0.5%)	365.271 (-2.3%)
<i>Exp</i> ($x=0.2$)	6.1551	6.1551	11.3990	373.999
LSDA ($x=0.1$)	6.0839 (-1.3%)	6.0839 (-1.3%)	11.9336 (+4.4%)	382.245 (+1.8%)
<i>Exp</i> ($x=0.1$)	6.1663	6.1663	11.3985	375.289

An analysis of Table 2 allows us to conclude that the theoretical LSDA+U approach give results with a reasonable approximation to the experimental data, as it can be obtained for $GdMnO_3$ (FERREIRA, 2018).

3.3 Partial Density of States

The Kohn-Sham electronic band structure gives a picture of the electronic eigenenergies E as a function of a wavevector k in the first Brillouin zone (BZ). The partial densities of states (PDOS) per orbital for the here studied $Y_{1-x}Eu_xMnO_3$ are shown individually in Fig. 3. The obtained PDOS are mainly formed from d atomic orbitals, particularly the bands between 0.0 and -1.0 eV.

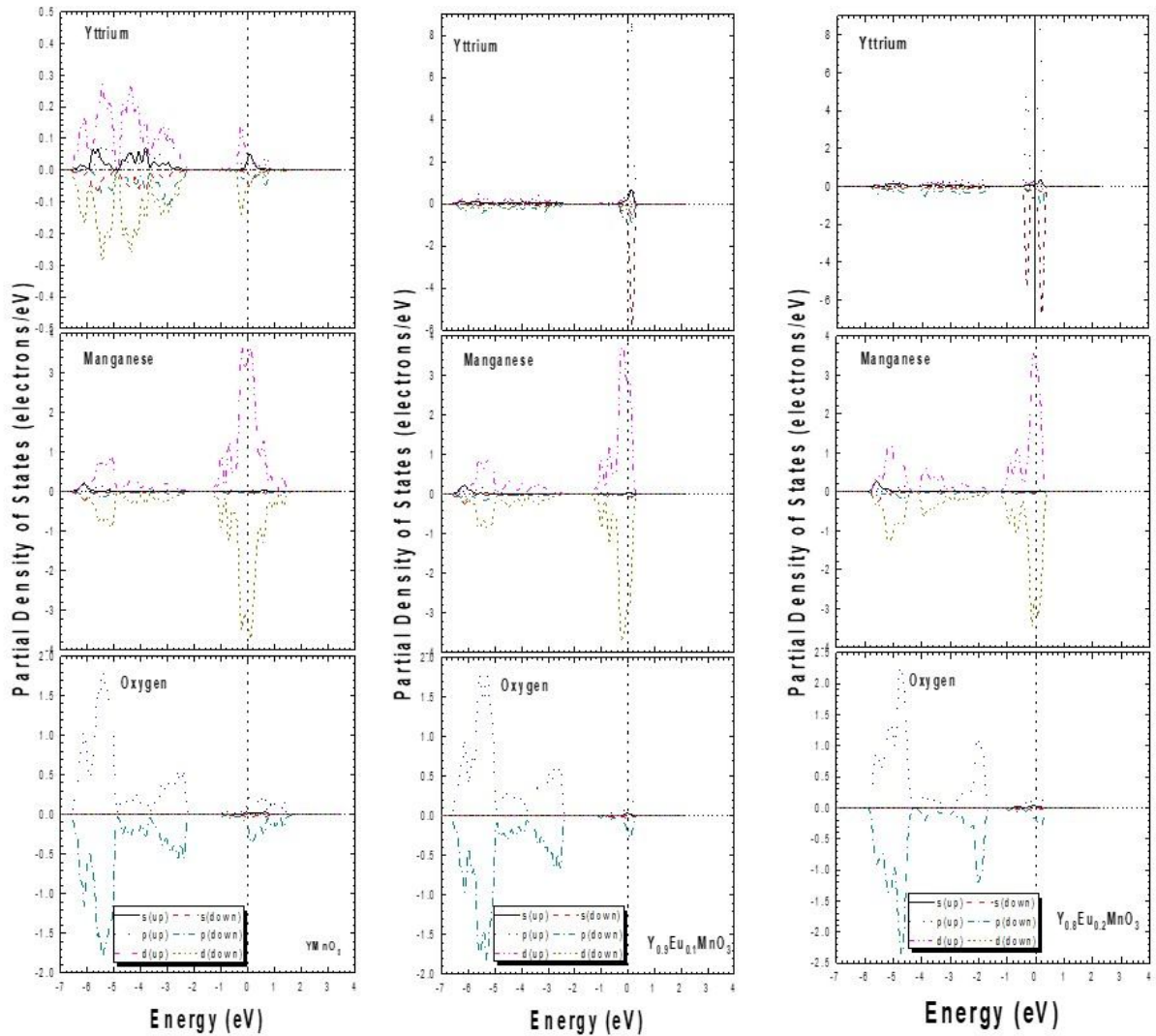


Fig. 3. Partial density of states of $Y_{1-x}Eu_xMnO_3$ recorded at room temperature.

The Fermi level is taken as 0.0 eV. For energy bands below the Fermi level, the smaller contribution, from the O-2p level. The main contribution observed around the Fermi level, is dominated by the orbitals from the transition metal element specifically the Mn-3d orbitals. This is important because manganese presents the magnetic characteristics.

PDOS analysis formalism is not for high energy states in the conduction band, in our case PDOS representation will usually decay to zero at about 1 eV above the Fermi level. This is associated with the fact that expansion of essentially free electron states in terms of a limited number of atomic-like basis functions is impossible to carry out with any degree of accuracy. Only the valence band and lower part of the conduction band are meaningful in the PDOS plot.

4. CONCLUSION

$Y_{1-x}Eu_xMnO_3$ perovskite were studied using a DFT formalism, based on the local density approximation (LSDA+U) for the exchange-correlation functional. After geometry optimization, we have obtained lattice parameters that compare well with experimental X-ray with the difference between calculated values and experiment being less than 2% because the LDA exchange- correlation energy tends to produce larger forces between atoms, an effect also responsible for the small lattice parameters (angles and bond length) predicted by using this level of theory in comparison with measurements.

The density of states at the Fermi level is dominated by Mn seems consistent with the fact that the system is ferroelectric. Finally, the calculated PDOS shows important contributions from the rare earth and the oxygen atoms in both systems, in which main contributions comes from the manganese atom.

REFERENCES

1. Kopyl S, Surmenev R, Surmeneva M, Fetisov Y, Kholkin A. Magnetolectric effect: principles and applications in biology and medicine – a review. *Materials Today Bio.* 2021; 12:100149. <https://doi.org/10.1016/j.mtbio.2021.100149>
2. Xu L, Liu Q, Meng J, Liao W, Liu X, Zhang H. Eu–Mn charge transfer and the strong charge–spin–electronic coupling behavior in $EuMnO_3$. *Inorg. Chem.* 2021; 60, 3: 1367-1379. <https://doi.org/10.1021/acs.inorgchem.0c02498>
3. Ferreira WS, Moreira JA, Almeida A, Chaves MR, Araújo JP, Oliveira JB, Silva JMM, Sá MA, Mendonça TM, Carvalho PS, Kreisel J, Ribeiro JL, Vieira LG, Tavares PB, and Mendonça S. Spin-phonon coupling and magnetolectric properties: $EuMnO_3$ versus $GdMnO_3$. *Phys. Rev. B* 2009; 79: 054303. <https://doi.org/10.1103/PhysRevB.79.054303>
4. Ferreira WS, Moreira JA, Almeida A, Araújo JP, Mendonça TM, Carvalho PS, Tavares PB, and Mendonça S. Dielectric and magnetic properties of $ReMnO_3$ (Re=Eu, Gd) ceramics. *Ferroelectrics.* 2008; 368: 107-113. <https://doi.org/10.1080/00150190802368065>
5. Moreira JA, Almeida A, Ferreira WS, Araújo JE, Pereria AM, Kreisel J, Vilela SMF, Tavares PB. *Phys. Rev. B.* 2010; 81: 054447. <https://doi.org/10.1103/PhysRevB.81.054447>
6. Mota D, Barcelay YRX, Tavares P, Chaves MR, Almeida A, Oliveira J, Ferreira WS and Moreira JAG. Competing exchanges and spin–phonon coupling in $Eu_{1-x}R_xMnO_3$ (R=Y, Lu). *J. Phys. Cond. Matt.* 2013; 25: 235602. <https://doi.org/10.1088/0953-8984/25/23/235602>
7. Ferreira WS, Moreira JAG, Almeida A, Chaves MR, Vilela S, Tavares P, Kundys B, Ranjith R and Prellier W. Effect of the external fields on the polar and dielectric properties of $Eu_{0.8}Y_{0.2}MnO_3$. *J. App. Phys.* 2010; 107: 024108. <https://doi.org/10.1063/1.3291122>
8. Hohenberg P, Kohn W. *Phys. Rev. B.* 1964; 136: 864.
9. Kohn W, Sham LJ. *Phys. Rev. A* 1965; 140: 1133.
10. Segall MD, Lindan PLD, Probert MJ, Pickard CJ, Hasnip PJ, Clark SJ, and Payne MC. First-principles simulation: ideas, illustrations and the CASTEP code. *J. Phys.: Condens. Matter.* 2002; 14: 2717. <https://doi.org/10.1088/0953-8984/14/11/301>
11. Ferreira WS, Moreira E, Frazão N. Mott Transition in $GdMnO_3$: an ab initio study. *Braz. J. Phys.* 2018; 48: 126-129. <https://doi.org/10.1007/s13538-018-0555-y>
12. Perdew J, Zunger A. Self-interaction correction to density-functional approximations for many-electron systems. *Phys. Rev. B.* 1981; 23: 5048-5079. <https://doi.org/10.1103/PhysRevB.23.5048>
13. Cerpeley DM, Alder BJ. Ground state of the electron gas by a stochastic method. *Phys. Rev. Lett.* 1980; 45: 566-569. <https://doi.org/10.1103/PhysRevLett.45.566>

14. Vanderbilt D. Soft self-consistent pseudopotentials in a generalized eigenvalue formalism Phys. Rev. B. 1990; 41: 7892-7895. <https://doi.org/10.1103/PhysRevB.41.7892>
15. Wilson DJ, Winkler B, Juarez-Arellano EA, Friedrich A, Knorr K, Pickard CJ, Milman V. Virtual crystal approximation study of nitridosilicates and oxonitridoaluminosilicates J. Phys. Chem. Sol. 2008; 69: 1861. <https://doi.org/10.1016/j.jpcs.2008.01.009>
16. Monkhorst HJ, Pack JD. Special points for Brillouin-zone integrations Phys. Rev. B. 1976; 13: 5188-5192. <https://doi.org/10.1103/PhysRevB.13.5188>
17. Pfromer B G, Côté M, Louie SG, Cohen ML. Relaxation of Crystals with the Quasi-Newton Method J. Comp. Phys. 1997; 131: 233-240. <https://doi.org/10.1006/jcph.1996.5612>

UNDER PEER REVIEW